EasyChair Preprint

№ 13317

A Wide Power Range Segment Control and Soft-Switching Implementation Method Based on AVC-VF Control

Yuhong Mo, Jing Xiao, Xiaoyu Zhu, Shaonan Chen and Xiaorui Wu

May 16, 2024

A Wide Power Range Segment Control and Soft-Switching Implementation Method Based on AVC-VF Control

Yuhong Mo [1, 2]
1 Southern Power Grid Corporation Wireless Power Transmission Joint Laboratory
2 Electric Power Research Institute of Guangxi Power Grid Co.,Ltd
Nanning, China
Email: 283581817@qq.com

Jing Xiao[1, 2]*
1 Southern Power Grid Corporation Wireless Power Transmission Joint Laboratory
2 Electric Power Research Institute of Guangxi Power Grid Co.,Ltd
Nanning, China
Email: 442756088@qq.com

Xiaoyu Zhu
College of Automation
Chongqing University
Chongqing, China
Email: 251328984@qq.com

Shaonan Chen [1, 2]
1 Southern Power Grid Corporation Wireless Power Transmission Joint Laboratory
2 Electric Power Research Institute of Guangxi Power Grid Co.,Ltd
Nanning, China
Email: 451310528@qq.com

Xiaorui Wu[1, 2]
1 Southern Power Grid Corporation Wireless Power Transmission Joint Laboratory
2 Electric Power Research Institute of Guangxi Power Grid Co.,Ltd
Nanning, China
Email: hiung@qq.com

Abstract – When EV-WPT system outputs in a wide range, the inverter runs in the non-soft switching region and the control stability is poor. Aiming at this problem, this paper studies the soft-switching control strategy of inverter under wide power range output, gives a segment control method based on asymmetric voltage cancellation-variable frequency (AVC-VF) control, establishes the model of EV-WPT system and analyzes its characteristics. A segment control method to realize wide-range output is given, and the conditions for the inverter to realize ZVS under the control of this method are given. According to this condition, a segment control method based on AVC-VF control is proposed, which can realize the wide-range output of the system and keep the soft-switching operation of the inverter, effectively reduce the energy loss of the inverter, thus improving the system efficiency. In addition, the method is verified by simulation.

keywords – EV-WPT , LCC-S resonant compensation topology, Soft-switching technology, AVC-VF control.

I. INTRODUCTION

Electric vehicle wireless power transfer (EV-WPT) technology can avoid many disadvantages of wired charging. It uses wireless power transmission (WPT) technology to transmit the power of the power grid to the electrical equipment in a non-electrical contact mode. The reference source was not found. At present, the wireless charging technology mainly has electric-field coupling wireless power transfer (EC-WPT) technical errors! The reference source was not found. And magnetic coupling wireless power transfer (MC-WPT) technology. Because MC-WPT technology can realize long distance, large capacity and high efficiency power transmission, EV-WPT system is usually realized by MC-WPT technology.

A typical EV-WPT system is shown in Figure 1. The whole charging equipment is divided into a transmitter and a receiver. The transmitter is located underground and is responsible for converting the electric energy of the power grid into high-frequency alternating current and transmitting it to the receiver through the transmitter coil. The receiver is assembled on an electric vehicle and is responsible for converting the high-frequency alternating current transmitted from the transmitter into electric energy and storing it in the battery. During the whole charging process of EV-WPT system, from the initial AC power to the energy storage in the battery, it involves many times of conversion and transmission of electric energy. In addition, EV-WPT system adopts high-frequency working mode, which will inevitably produce a lot of energy loss in the converter, which will not only reduce the overall efficiency, but also increase the cooling demand of the system and affect the service life of components. Therefore, it is necessary to reduce the converter loss, thus reducing the system heat and improving the overall efficiency of the system. In EV-WPT system, the application of soft switching technology can effectively solve this problem.

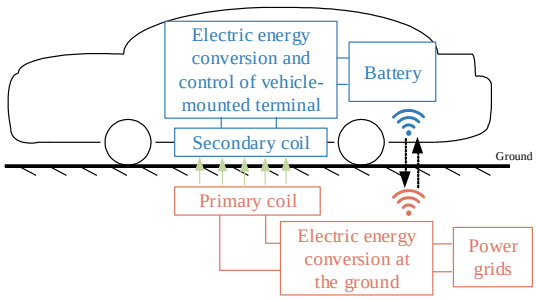

Fig. 1 Schematic diagram of EV-WPT system

Compared with the design of resonant element parameters and the addition of auxiliary network to realize ZVS, the control strategy can reduce the number of elements in the circuit, simplify the structure of the whole system, reduce the cost and volume, and can be adjusted and optimized according to actual needs to meet the requirements of different working conditions. At present, many different modulation strategies have been proposed for inverter ZVS, including Pulse Frequency Modulation (PFM), Pulse Width Modulation (PWM) and hybrid control.

For pulse frequency control, documents [1]-[4] realize output regulation and ZVS by adjusting the switching frequency of converters. When PFM control is applied to a wide output range, it needs a wide switching frequency range to meet the requirements of system voltage gain. However, when the switching frequency range of the system is large, soft switching may be lost, and the system efficiency will become low, in addition, it will cause electromagnetic interference.

Pulse width control includes Phase Shift (PS) control, Asymmetrical Duty-Cycle (ADC) control and asymmetric voltage cancellation (AVC) control. Based on phase shift control, references [5]-[8] realize the adjustment of output voltage by adjusting phase shift angle, although PS control can achieve a wide range of output voltage gain. Asymmetric duty control [9]-[10] and asymmetric voltage cancellation control [11]-[13] adjust the output voltage by adjusting the pulse width of the driving signal of the full-bridge inverter, but it is not easy to realize soft switching when the demand for output voltage gain range is large.

When the traditional control strategy can't meet the requirements of the system, the hybrid control strategy is often adopted. For example, when the system needs to realize ZVS in a wide output range, a single PFM or PWM control can't be realized. In order to solve this problem, references [14]-[17] adopt the frequency conversion-phase shift control method to realize ZVS operation in a wide output range.

By optimizing the soft-switching control strategy, a faster and more stable charging process can be realized, and the energy utilization rate can be improved. Because the energy consumption and heat generation of the system are reduced, the service life of system components can be prolonged, and the maintenance and replacement costs can be reduced. The organizational structure of this paper is as follows. In the second part, the system model is established and its transmission characteristics are analyzed. In the third part, a subsection control method based on AVC-VF control is proposed, and the conditions for the inverter to realize ZVS under its control are analyzed, and the specific implementation method is given. The fourth part builds a simulation model to verify the effectiveness of the proposed method.

II. System Configuration And Characteristics Analysis

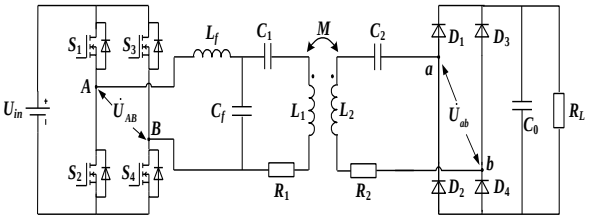

Fig. 2 Circuit diagram of LCC-S EV-WPT system

Fig. 2 is the circuit diagram of LCC-S EV-WPT system, in which $S_1 \sim S_4$ is MOSFET switch, $D_1 \sim D_4$ is rectifier diode, U_{in} is DC voltage source, $\dot{U}_{AB}$ is inverter output voltage, L_f is transmitter compensation inductance, C_f and C_1 are transmitter parallel compensation capacitance and series compensation capacitance respectively, L_1 is transmitter coil, L_2 is receiver coil, C_2 is receiver series compensation capacitance, C_0 is receiver filter capacitance, and M is mutual inductance between transmitter coil and receiver coil. $\dot{U}_{ab}$ is the rectified terminal voltage, R_L is the equivalent load of the system, R_1 and R_2 are the internal resistances of the transmitting coil and the receiving coil respectively.

The equivalent impedance before the load is converted to the rectifier bridge is:

$$R_L^{'} = \frac{8}{\pi^2} R_L \tag{1}$$

ω_s is the switching angular frequency of the inverter, so that the resonant angular frequency of the system is ω_0. When the system meets the resonance condition, there is the following relationship:

$$\begin{cases} \omega_0 L_f = \dfrac{1}{\omega_0 C_f} \\ \omega_0 L_1 - \omega_0 L_f = \dfrac{1}{\omega_0 C_1} \\ \omega_0 L_2 = \dfrac{1}{\omega_0 C_2} \end{cases} \tag{2}$$

The available equivalent reflection impedance is:

$$Z_{ref} = \frac{\omega_0^2 M^2}{j\omega_0 L_2 + \dfrac{1}{j\omega_0 C_2} + R_L^{'}} = \frac{\omega_0^2 M^2}{R_L^{'} + R_2} \tag{3}$$

The input impedance of the system compensation network is:

$$Z_{in} = \frac{\omega_0^2 L_f^2 (R_L^{'} + R_2)}{\omega_0^2 M^2 + R_1 R_L^{'} + R_1 R_2} \tag{4}$$

It can be obtained that the current expression of each branch is:

$$\begin{cases} \dot{I}_{Lf} = \dfrac{\dot{U}_{AB}}{Z_{in}} \\ \dot{I}_1 = \dfrac{j\omega_0 L_f \dot{U}_{AB}}{(R_1 + \dfrac{\omega_0^2 M^2}{R_L' + R_2}) Z_{in}} \\ \dot{I}_{Cf} = \dfrac{(j\omega_0 L_f + R_1 + \dfrac{\omega_0^2 M^2}{R_L' + R_2}) \dot{U}_{AB}}{\left(R_1 + \dfrac{\omega_0^2 M^2}{R_L' + R_2}\right) Z_{in}} \\ \dot{I}_2 = \dfrac{\omega_0^2 M L_f \dot{U}_{AB}}{(R_2 + R_L')(R_1 + \dfrac{\omega_0^2 M^2}{R_L' + R_2}) Z_{in}} \end{cases} \tag{5}$$

III. System Design

A. Realization of wide output power range

AVC control is a generalized inverter control method. Figure 3 is the waveform diagram of driving signal, output voltage and current of full-bridge inverter based on AVC control strategy. In which, $S_1 \sim S_4$ is the driving signal of four switches of the full-bridge inverter, T_s is the period of the driving signal of the switches, β is the half period of the switches, u_{AB} is the inverter output voltage, i_{Lf} is the inverter output current, α_+ and a_- are the adjustable control angles.

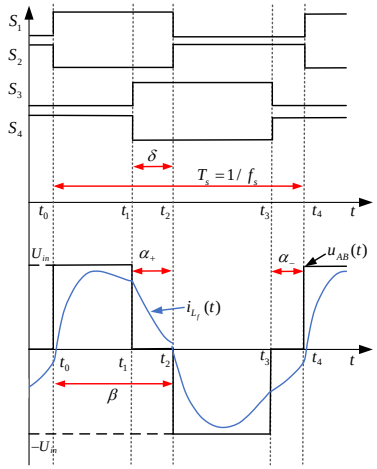

Fig. 3 AVC control waveform diagram

Based on the control waveform and inverter output voltage waveform in Figure 3, the piecewise expression of $u_{AB}(t)$ can be obtained as follows:

$$u_{AB}(t)=\begin{cases} U_{in} & t_0 \le t \le t_1 \\ 0 & t_1 < t \le t_2 \\ -U_{in} & t_2 < t \le t_3 \\ 0 & t_3 < t < t_4 \end{cases} \tag{6}$$

where $t_0 - t_4$ is the moment when the switch tube is turned on and off, and there is the following relationship:

$$\begin{cases} \omega_s t_0 = 0 \\ \omega_s t_1 = \beta - \alpha_+ \\ \omega_s t_2 = \beta \\ \omega_s t_3 = \omega_s T_s - \alpha_- \\ \omega_s t_4 = \omega_s T_s \end{cases} \tag{7}$$

The time domain expression of the inverter output voltage can be expressed by Fourier series as follows: $|U_{AB}|$ is the amplitude of the inverter output voltage, φ_N is the phase of the inverter output voltage, and N is the harmonic number:

$$u_{AB}(t)=\sum_{N=1}^{\infty}|U_{ABN}|\sin(N\omega_s t+\varphi_N) \tag{8}$$

among them:

$$\begin{cases} |U_{ABN}| = \dfrac{U_{in}}{N\pi}\sqrt{a_N^2+b_N^2} \\ \varphi_N = \arctan\dfrac{a_N}{b_N} \end{cases} \tag{9}$$

$$\begin{cases} a_N = \sin(N(\beta-\alpha_+))+\sin(N\beta)+\sin(N\alpha_-) \\ b_N = 1-\cos(N(\beta-\alpha_+))-\cos(N\beta)+\cos(N\alpha_-) \end{cases} \tag{10}$$

According to the above analysis, the expression of φ_N can be obtained as follows:

$$\varphi_N = \arctan\frac{\sin(N(\beta-\alpha_+))+\sin(N\beta)+\sin(N\alpha_-)}{1-\cos(N(\beta-\alpha_+))-\cos(N\beta)+\cos(N\alpha_-)} \tag{11}$$

According to the different values of the three control variables, there are several commonly used typical control strategies. When $\delta=\alpha_+$, $\alpha_-=0$, $\beta=180°$ is the optimal asymmetric voltage cancellation control (OAVC control), when $\delta=\alpha_+=\alpha_-$ and $\beta=180°$ is the phase shift control (PS control).

Substitute the constraints of the two control strategies into Equation (9), (10) and(11), we can get that for OAVC control:

$$\begin{cases} a_N = \sin(N\delta) \\ b_N = 3+\cos(N\delta) \\ \varphi_N = \arctan\dfrac{\sin(N\delta)}{3+\cos(N\delta)} \\ |U_{ABN}| = \dfrac{U_{in}}{N\pi}\sqrt{10+6\cos(N\delta)} \end{cases} \tag{12}$$

For PS control:

$$\begin{cases} a_N = 2\sin(N\delta) \\ b_N = 2+2\cos(N\delta) \\ \varphi_N = \dfrac{N\delta}{2} \\ |U_{ABN}| = \dfrac{4U_{in}}{N\pi}\cos(\dfrac{N\delta}{2}) \end{cases} \tag{13}$$

P_L^* is defined as normalized output power, we can get the expression of P_L^* as follows:

$$P_L^* = \frac{P_L}{P_{E-\text{load}}} = \frac{|I_{Lf}|^2\,\mathrm{Re}(Z_{in})}{\dfrac{8M^2U_{in}^2}{\pi^2 L_f^2 R_L'}} \tag{14}$$

When the control strategy of the inverter is OAVC control, the range of the normalized output power of the inverter is between 0.25 and 1. It can be seen that the output power gain of the inverter cannot be between 0 and 0.25 by OAVC control, and the control strategy needs to be changed if the output power gain is between 0 and 0.25. On this basis, adjusting A and B at the same time, and when A and B are not equal to 0, the output power gain can be between 0 and 0.25. In order to simplify the design of the controller, A can be equal to B, which is the traditional phase-shifting control. Therefore, in order to realize the wide power range output of the system and maintain high efficiency during the system operation, this paper presents a subsection control strategy based on AVC control. When the normalized output power of the inverter is between 0 and 0.25, PS control is adopted, and when the output power gain varies between 0.25 and 1, OAVC control is adopted, as shown in Figure 3.

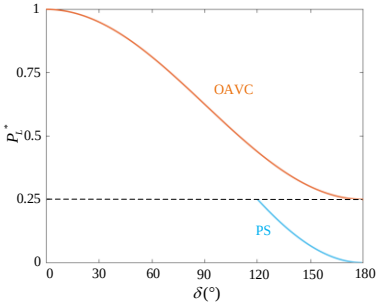

Fig. 3 Curve of relationship between and control angle under the Segment control

Combined with the charging process of EV-WPT system, the system runs in the range of 0.25 to 1 for a long time. In this range, using OAVC control can realize ZVS operation in a small switching frequency range, which can effectively improve the system efficiency. Both OAVC control and PS control belong to the generalized control

method-AVC control. Therefore, the conditions for realizing soft switching under AVC control can be deduced to realize the segmented control method of OAVC+PS to realize ZVS under wide power range output.

B. Soft-switching operating condition

Compared with the fundamental wave and the third harmonic wave, the fifth and above harmonic components have less influence on the system[18]. Therefore, this paper only considers the fundamental wave and the third harmonic, and the vector form of $u_{C_f}(t)$ is as follows:

$$\dot{U}_{C_f N} = \left|U_{C_f N}\right| \angle \varphi_{U_{C_f N}}, N = 1,3 \tag{15}$$

Based on Thevenin-Norton theorem, the equivalent circuit diagram of the system is simplified as shown in Figure 4. Where $\dot{I}_{eqN}$ is the equivalent input current source, Z_{eqN} is the equivalent impedance, C_{eqN} and L_{eqN} are the equivalent capacitance of the combination of L_f and C_f and the equivalent inductance of the combination of L_1 and C_1 under the N-th harmonic respectively.

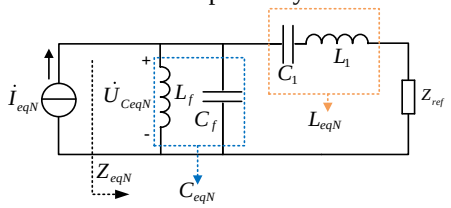

Fig. 4 Simplified equivalent circuit diagram

C_{eqN} and L_{eqN} can be expressed as follows:

$$\begin{cases} C_{eqN} = \dfrac{N^2\omega_s^2 L_f C_f - 1}{N^2\omega_s^2 L_f} \\ L_{eqN} = \dfrac{N^2\omega_s^2 L_1 C_1 - 1}{N^2\omega_s^2 C_1} \end{cases} \tag{16}$$

According to $u_{L_f}(t) = u_{AB}(t) - u_{C_f}(t) = L_f\left(di_{L_f}(t)/dt\right)$, the expression of $i_{L_f}(t)$ can be obtained:

$$i_{L_f}(t) = \begin{cases} \dfrac{1}{\omega_s L_f}\left\{U_{in}\omega_s t + \sum_{N=1}^{3}\left[\dfrac{\sqrt{2}\,\mathrm{Re}(\dot{U}_{C_{eqN}})}{N}\cos(N\omega_s t+\varphi_N) - \dfrac{\sqrt{2}\,\mathrm{Im}(\dot{U}_{C_{eqN}})}{N}\sin(N\omega_s t+\varphi_N)\right]\right\} + h_0, & t_0 \le t \le t_1 \\ \dfrac{1}{\omega_s L_f}\left\{\sum_{N=1}^{3}\left[\dfrac{\sqrt{2}\,\mathrm{Re}(\dot{U}_{C_{eqN}})}{N}\cos(N\omega_s t+\varphi_N) - \dfrac{\sqrt{2}\,\mathrm{Im}(\dot{U}_{C_{eqN}})}{N}\sin(N\omega_s t+\varphi_N)\right]\right\} + h_1, & t_1 \le t \le t_2 \\ \dfrac{1}{\omega_s L_f}\left\{-U_{in}\omega_s t + \sum_{N=1}^{3}\left[\dfrac{\sqrt{2}\,\mathrm{Re}(\dot{U}_{C_{eqN}})}{N}\cos(N\omega_s t+\varphi_N) - \dfrac{\sqrt{2}\,\mathrm{Im}(\dot{U}_{C_{eqN}})}{N}\sin(N\omega_s t+\varphi_N)\right]\right\} + h_2, & t_2 \le t \le t_3 \\ \dfrac{1}{\omega_s L_f}\left\{\sum_{N=1}^{3}\left[\dfrac{\sqrt{2}\,\mathrm{Re}(\dot{U}_{C_{eqN}})}{N}\cos(N\omega_s t+\varphi_N) - \dfrac{\sqrt{2}\,\mathrm{Im}(\dot{U}_{C_{eqN}})}{N}\sin(N\omega_s t+\varphi_N)\right]\right\} + h_3, & t_3 \le t \le t_4 \end{cases} \tag{17}$$

where $N = 1,3$, $h_0 - h_2$ is the constant term of each piecewise function, which is determined by the circuit parameters. Because of the continuity of inductance current, the piecewise expression of $i_{L_f}(t)$ should be equal from beginning to end, and we can get:

$$\begin{cases} h_1 = \dfrac{U_{in}(\beta - \alpha_+)}{\omega_s L_f} + h_0 \\ h_2 = \dfrac{U_{in}(2\beta - \alpha_+)}{\omega_s L_f} + h_0 \\ h_3 = \dfrac{U_{in}(2\beta - \alpha_+ - \omega_s T_s + \alpha_-)}{\omega_s L_f} + h_0 \end{cases} \tag{18}$$

The integral of $i_{L_f}(t)$ in the period T_s is zero:

$$\int_{t_0}^{t_4} i_{L_f}(t)dt = 0 \tag{19}$$

The following can be obtained:

$$h_0 = \frac{U_{in}\left[(\beta-\alpha_+)^2 - (\omega_s T_s - \alpha_-)\omega_s T_s\right]}{-2\omega_s{}^2 T_s L_f} - \frac{U_{in}[\beta^2 + (\alpha_+ + \omega_s T_s)(2\beta - \alpha_+)]}{-2\omega_s{}^2 T_s L_f} \tag{20}$$

According to Figure 3, it can be known that in order to realize soft switching of full-bridge inverter, the voltage on the parasitic capacitor of the switching tube needs to be exhausted before the switching tube is turned on, so the following conditions need to be met in order to realize soft switching:

$$\begin{cases} i_{L_f}(t_0) \le -I_{op} \\ i_{L_f}(t_1) \ge I_{op} \\ i_{L_f}(t_2) \ge I_{op} \\ i_{L_f}(t_3) \le -I_{op} \end{cases} \tag{21}$$

where I_{op} is the operating current of the switch tube on and off, which is used to discharge the parasitic capacitance of the switch tube.

Add $i_{L_f}(t_0)$ and $i_{L_f}(t_1)$ to get:

$$i_{L_f}(t_0) + i_{L_f}(t_1) = \frac{2\sin\delta}{\sqrt{1+\cos\delta}}\left|\mathrm{Im}(\dot{U}_{ceq1})\right| + \frac{2\sin(3\delta)}{\sqrt{1+\cos(3\delta)}}\left|\mathrm{Im}(\dot{U}_{ceq3})\right| \tag{22}$$

When the angle $0 \le \delta < \pi/3$ or $2\pi/3 \le \delta < \pi$ is controlled, $i_{L_f}(t_0) + i_{L_f}(t_1) \ge 0$, when $\pi/3 \le \delta < 2\pi/3$, the first term on the right side of the above formula is positive, and the second term is not positive. However, since` $\left|\mathrm{Im}(\dot{U}_{ceq3})\right|$ is far less than $\left|\mathrm{Im}(\dot{U}_{ceq1})\right|$, there is still $i_{L_f}(t_0) + i_{L_f}(t_1) \ge 0$. Combining with the ZVS realization condition, it can be obtained that when $i_{L_f}(t_0) \le -I_{op}$, $i_{L_f}(t_1) \ge I_{op}$ must be established, and when $i_{L_f}(t_2) \ge I_{op}$ can be obtained in the same way, $i_{L_f}(t_3) \le -I_{op}$ is established, so the soft switching realization condition can be simplified as:

$$\begin{cases} i_{L_f}(t_0) \le -I_{op} \\ i_{L_f}(t_2) \ge I_{op} \end{cases} \tag{23}$$

Parameter drift may occur in the practical application of the system, and a margin of 5% is reserved when setting the soft-switching realization conditions, so the conditions for the inverter to realize ZVS are as follows:

$$\begin{cases} 95\% i_{L_f}(t_0) \le -I_{op} \\ 95\% i_{L_f}(t_2) \ge I_{op} \end{cases} \tag{24}$$

C. Segment control strategy and implementation based on AVC-VF control

According to the expression of $i_{L_f}(t)$ obtained above, we can get the changing trends under the control of OAVC and PS respectively and between the normalized frequency and the control angle, as shown in Figure 5 and Figure 6. As can be seen from the figure, no matter how much the control angle is, the value of a monotonically increases with f_s^*. Therefore, ZVS conditions can be used to adjust the switching frequency to realize the ZVS operation of the inverter.

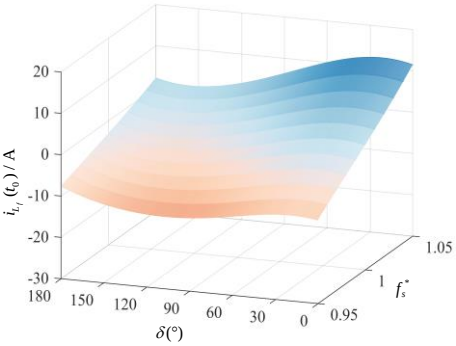

Fig. 5 Relationship between $i_{L_f}(t_0)$ and control angle δ and normalized frequency f_s^* under the OAVC control

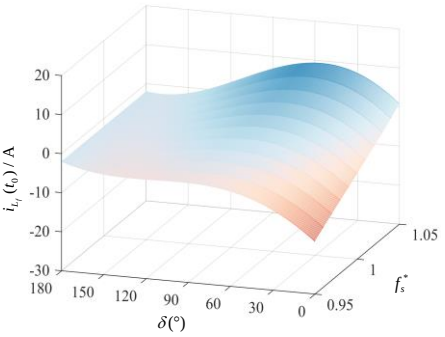

Fig. 6 Relationship between $i_{L_f}(t_0)$ and control angle δ and normalized frequency f_s^* under the PS control

In addition to adjusting the control angle δ and switching frequency f_s to achieve the operating conditions of soft switching, it is also necessary to meet the condition that the adjustment range of f_s is as small as possible, so as to maintain the efficient operation of the system. Fig. 7 shows the optimal operation trajectory of the inverter to realize ZVS. The region ABCE and the region FBDE are based on ZVS realization conditions, and the intersection of the two regions is the region where the inverter can realize ZVS operation, as shown in the figure, region 1 (region FBCE). Point A is the rated operating point of the system. At this time, the control angle is 0 and the switching frequency is equal to the system resonance frequency. In order to ensure the efficient operation of the system, the change of the switching frequency should be as small as possible. Therefore, the red dotted line in the figure is the optimal operation curve of inverter ZVS. When it is necessary to reduce the output power of the system, first keep the switching frequency unchanged and increase the control angle δ, that is, the system runs along ab. At this time, the system runs in area 1; After reaching the critical point B, if the output power still needs to be reduced, only adjusting the control angle δ will make the system run in the non-soft switching area, that is, the system will run along the BE.

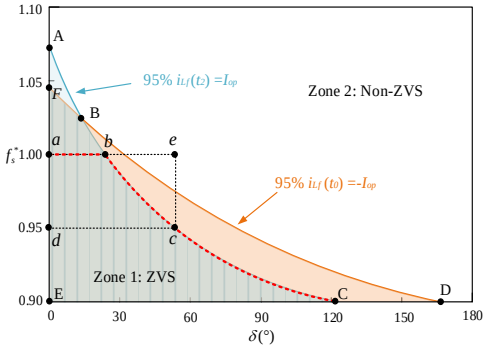

Fig. 7 Relationship between $i_{L_f}(t_0)$ and control angle δ and normalized frequency f_s^* under the OAVC control

If the system is to run in the soft switching area, then it is necessary to adjust fs on the basis of adjusting δ to make the operating point run along the red dotted line until the desired output power is reached. In addition, when the control angle q increases, if the switching frequency is not adjusted, the inverter will run along the cd. At this time, although the system runs in the soft switching area, the switching frequency deviates from the resonant frequency at this time. Therefore, it is necessary to adjust the switching frequency at the same time to make the inverter run along the cba.

Through the above analysis, we can know that the system can realize soft switching in a wide range of power changes and maintain high efficiency by making the operating point run along the optimal working trajectory, and the above control strategy is called AVC-VF control.

IV. Simulation Verification

The soft-switching in the wide power range of the system is verified, and the simulation model is built in Matlab/simulink, and the inverter output voltage and current waveform diagram shown in Figure 8 can be obtained.

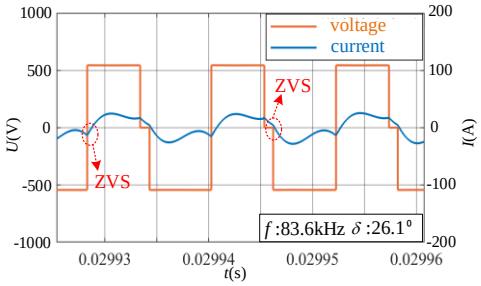

(a) 7/8 P_L(OAVC-VF control)

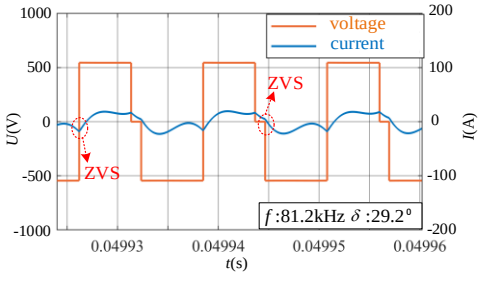

(b) 5/8 P_L(OAVC-VF control)

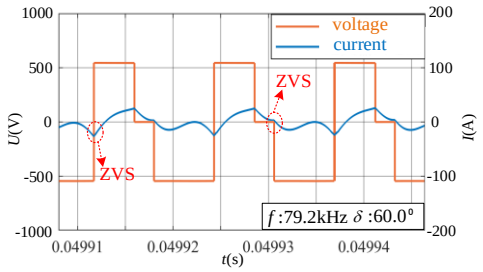

(c) 3/8 P_L(OAVC-VF control)

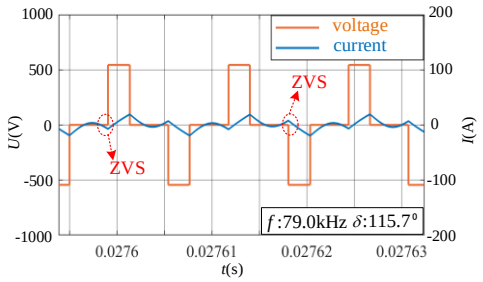

(d) 1/8 P_L(PS-VF control)

Fig. 8 The waveform of inverter output voltage and current

Figure 8 shows the voltage and current waveforms of the inverter output when the normalized output power of the system is 7/8, 5/8, 3/8 and 1/8. It can be seen from the figure that when the normalized output power of the system is between 0.25 and 1, the OAVC-VF control strategy proposed in this paper is adopted, so that the system can realize ZVS operation while adjusting the output power, and the change range of switching frequency is small; When the normalized output power of the system is between 0 and 0.25, the ZVS operation of the four switches of the inverter can be realized by using PS-VF control strategy. From the simulation results, it can be seen that the proposed control method can realize the ZVS operation of the full-bridge inverter while adjusting the output power of the system.

V. Conclusion

In this paper, the wide power range output of EV-WPT system and the realization of soft switching of full-bridge inverter in wide power range are studied, and a segmented control strategy based on AVC-VF control is given, which realizes the wide power range ZVS realization of EV-WPT system full-bridge inverter and system output adjustment. The closed-loop control simulation model of EV-WPT system is established, and the ZVS realization characteristics of the system are verified. The simulation results show that the segmented control strategy based on AVC-VF control given in this paper can realize ZVS in a wide power range, and the feasibility of the given control method is verified.

Acknowledgment

Thanks for the support by Key Technology Project of China Southern Power Grid Corporation (GXKJXM20222143).

VI. Reference

[1] Deng P, Tang C, Fan Y, et al. A frequency regulation strategy for dynamic process noise suppression in LCC-S WPT systems[J]. IEEE Transactions on Power Electronics, 2022, 37(11): 13978-13988.

[2] Meng Y, Sun J, Duan Z, et al. Variable voltage variable frequency modular multilevel AC/AC converter with high-frequency harmonics filtering capability[J]. IEEE Journal of Emerging and Selected Topics in Power Electronics, 2021, 10(1): 811-821.

[3] Chen T, Yu R, Huang A Q. Variable-switching-frequency single-stage bidirectional GaN AC–DC converter for the grid-tied battery energy storage system[J]. IEEE Transactions on Industrial Electronics, 2021, 69(11): 10776-10786.

[4] Chen J, Sha D, Zhang J, et al. An SiC MOSFET based three-phase ZVS inverter employing variable switching frequency space vector PWM control[J]. IEEE Transactions on Power Electronics, 2018, 34(7): 6320-6331.

[5] Abbasi M, Emamalipour R, Cheema M A M, et al. A constant-frequency high-voltage gain resonant converter module with semiactive phase-shifted voltage multiplier for MVdc distribution[J]. IEEE Journal of Emerging and Selected Topics in Power Electronics, 2021, 10(4): 3603-3616.

[6] Liu X, Gao F, Zhang Y, et al. A multi-inverter high-power wireless power transfer system with wide ZVS operation range[J]. IEEE Transactions on Power Electronics, 2022, 37(12): 14082-14095.

[7] Sun X, Li X, Shen Y, et al. Dual-bridge LLC resonant converter with fixed-frequency PWM control for wide input applications[J]. IEEE Transactions on Power Electronics, 2016, 32(1): 69-80.

[8] Zhu G, Dong J, Shi W, et al. A mode-switching based phase shift control for optimized efficiency and wide ZVS operations in wireless power transfer systems[J]. IEEE Transactions on Power Electronics, 2023, 38(04): 5561-5575.

[9] Zong S, Luo H, Li W, et al. Asymmetrical duty cycle-controlled LLC resonant converter with equivalent switching frequency doubler[J]. IEEE Transactions on Power Electronics, 2015, 31(7): 4963-4973.

[10] Asa E, Colak K, Bojarski M, et al. Asymmetrical duty-cycle and phase-shift control of a novel multiport CLL resonant converter[J]. IEEE Journal of Emerging and Selected Topics in Power Electronics, 2015, 3(4): 1122-1131.

[11] Zhang J, Zhao J, Zhang Y, et al. A wireless power transfer system with dual switch-controlled capacitors for efficiency optimization[J]. IEEE Transactions on Power Electronics, 2019, 35(6): 6091-6101.

[12] Burdio J M, Barragan L A, Monterde F, et al. Asymmetrical voltage-cancellation control for full-bridge series resonant inverters[J]. IEEE transactions on Power Electronics, 2004, 19(2): 461-469.

[13] Jiang L, Costinett D. A high-efficiency GaN-based single-stage 6.78 MHz transmitter for wireless power transfer applications[J]. IEEE Transactions on Power Electronics, 2018, 34(8): 7677-7692.

[14] Jiang Y, Wang L, Wang Y, et al. Analysis, design, and implementation of WPT system for EV's battery charging based on optimal operation frequency range[J]. IEEE Transactions on Power Electronics, 2018, 34(7): 6890-6905.

[15] Han W, Corradini L. Wide-range ZVS control technique for bidirectional dual-bridge series-resonant DC–DC converters[J]. IEEE Transactions on Power Electronics, 2019, 34(10): 10256-10269.

[16] Hu H, Cai T, Duan S, et al. An optimal variable frequency phase shift control strategy for ZVS operation within wide power range in IPT systems[J]. IEEE Transactions on Power Electronics, 2019, 35(5): 5517-5530.

[17] Xu Y, Yu Z, Chen J, et al. A variable frequency phase-shift modulation constant power control strategy for LCC resonant capacitor charging power supply[J]. IEEE Transactions on Industrial Electronics, 2022, 70(2): 1883-1893.

[18] Hu J, Zhao J, Cui C. A wide charging range wireless power transfer control system with harmonic current to estimate the coupling coefficient[J]. IEEE Transactions on Power Electronics, 2020, 36(5): 5082-5094.